DOI: 10.13009/EUCASS2019-565

Data analysis for damage identification in CFRP stiffened structures using guided Lamb waves with PZT sensors

Christian Luis Aguilar Redondo[1], Antonio Fernández López[1], Alfredo Güemes[1]
[1]Technical University of Madrid
[1]Plaza Cardenal Cisneros, 328040, Madrid, Spain.
c.aguilar@alumnos.upm.es; antonio.fernandez.lopez@upm.es; alfredo.guemes@upm.es

Abstract

One of the most promising technique for the improvement of structural design and operational services of aerospace structures is the damage detection and identification using an embedded sensor network, generally known as Structural Health Monitoring (SHM). This paper is focused on studying how elastic waves propagate in aerospace composite structures: composite panels reinforced with stiffeners. An experimental study has been performed using T-shape stiffeners, the most standard structural reinforcement solution. Active and passive data signal processing for damage detection and identification has been carried out at the laboratory where two different stiffened CFRP panels were instrumented with piezoelectric sensors.

1. Introduction

Over the past several years, aerospace engineers have been challenged to apply the Structural Health Monitoring (SHM) technique, studying how Lamb waves propagates along composite structures. T-shape stiffeners are widely used in aircraft structures, such stringer-stiffened panels, being one of the most frequent solutions for thin panel stiffening.

Lamb wave signal processing and its damage feature extraction is essential for SHM, as well as the development of autonomous systems for the continuous monitoring, inspection and damage detection of structures based on integrated sensor networks is crucial to reduce the high costs of maintenance operations and human labour.

The aim of this work is to analyse the propagation of Lamb waves on a CFRP plate with a T-shape stiffener. A good understanding of how lamb waves propagate through stiffeners on composite panels is needed for a better damage detection and identification in these kind of structures [1]. This study presents the use of Lamb waves for quantitative identification of damage in stiffened composite structures. A detailed study of signal generation, signal processing and damage diagnosis is presented.

2. Active monitoring

PZT can be used either as sensors or as actuators. In the active monitoring techniques, damage detection is based on the data analysis of the elastic waves propagated trough the structure and generated by a PZT acting as actuator. For small thickness plates, Lamb waves are a type of elastic waves that can travel over a long distance even in materials with a high attenuation ratio, such CFRP plates, and thus a broad area can be quickly examined [2-4]. A brief review of Lamb waves is described below.

2.1 Lamb waves

Lamb waves are the particular solution for thin plates solid wave propagation, their propagation characteristics vary with entry angle, excitation and structural geometry [5]. Plates support two infinite sets of Lamb wave modes, whose velocities depend on the relationship between wavelength and plate thickness. Lamb mode can be classified either symmetric or anti-symmetric.

DOI: 10.13009/EUCASS2019-565

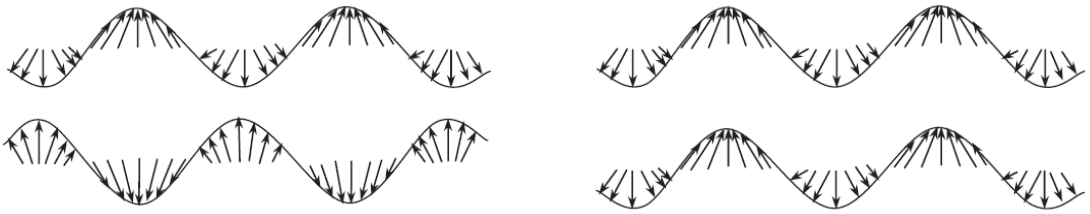

Figure 1: (a) Symmetric Lamb mode and (b) anti-symmetric Lamb mode

$$\frac{\tan(qh)}{\tan(ph)} = -\frac{4k^2qp}{(k^2-q^2)^2} \quad \textbf{(1a)}$$

$$\frac{\tan(qh)}{\tan(ph)} = -\frac{(k^2-q^2)^2}{4k^2qp} \quad \textbf{(1b)}$$

$$p^2 = -\frac{\omega^2}{C_L^2} - k^2, \qquad q^2 = -\frac{\omega^2}{C_T^2} - k^2, \quad \text{and} \quad k = {}^{\omega}/_{c_p} \quad \textbf{(2)}$$

where h, k, C_L, C_T, C_P, are the plate thickness, wavenumber, velocities of longitudinal and transverse modes, phase velocity and wave circular frequency, respectively. Eq. (1), correlating the propagation velocity with its frequency, implies that Lamb waves, regardless of mode, are dispersive (velocity is dependent on frequency).

In this particular case, for a composite structure with anisotropic properties, a complex phenomenon in wave propagation is introduced such as direction-dependent speed and difference between phase and group velocities.

2.2 Experimental setup

Two quasi-isotropic, 7-ply laminate of Hexcel AS4/8552 with the layup (+45, -45, 90, 0)$ resulting in a total thickness of 1.288 have been manufactured with (Fig. 2) and without a T-shape stiffener in its centre (Fig. 3). The stiffener has a symmetric 11-ply laminate of AS4/8552 with the layup: (+45, -45, 0, 0, 0, 90)$ which doubles on the central web, resulting in a thickness of 2.024 mm in the foot and 4.048 mm in the web.

Both panels have been instrumented with eight piezoelectric sensors at the same position. In order to analyze the effect of the Lamb waves propagation through the T-shape stiffener, the signals received in all the PZT sensors have been compared tracking all the possible ways.

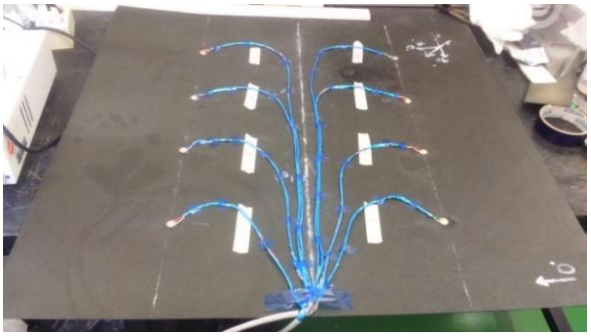

Figure 2: Flat panel (without T-shape stiffener)

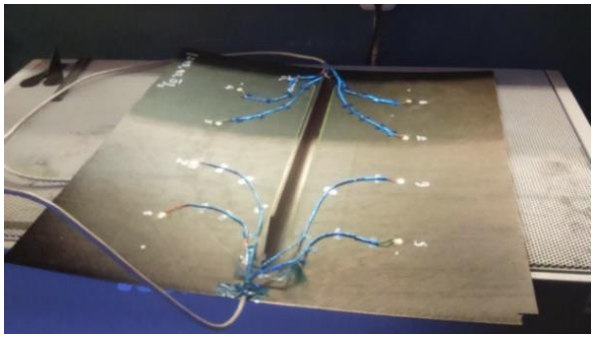

Figure 3: Panel with T-shape stiffener

DOI: 10.13009/EUCASS2019-565

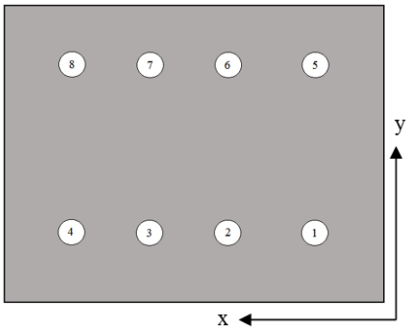

Figure 4: PZT positions in Flat panel.

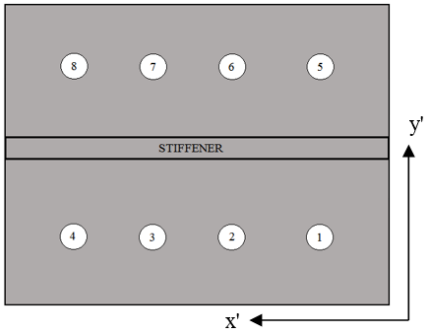

Figure 5: PZT positions in panel with T-shape stiffener.

A total of 7 signal ways can be collected from a single sensor. For a frequency range between 50 kHz and 500 kHz with a 50 kHz step and combining all possible emitting and receiving ways, a total of 560 signals are available in this experiment. A burst signal with three cycles has been chosen for all the analyses. The three peak signal emitted in the time domain and the Fast Fourier Transformation (FFT) of the generated signal are shown in Fig. 6.a and Fig. 6.b.

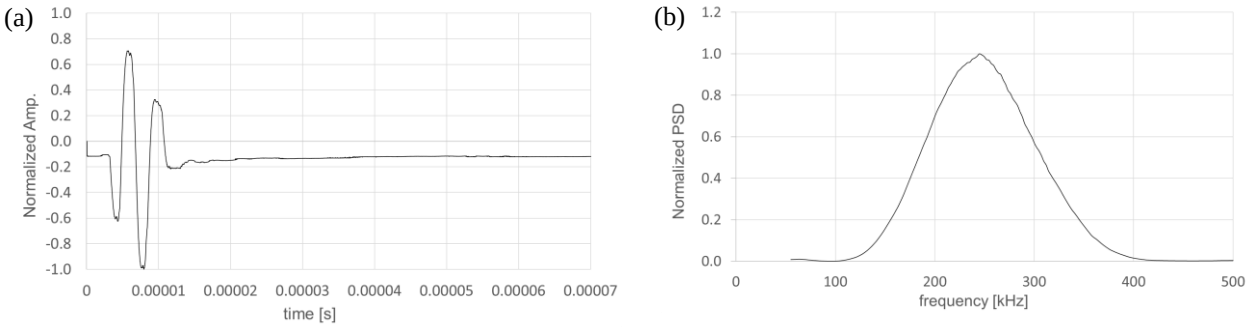

Figure 6: (a) 3 peaks burst signal at 250 kHz in time domain and (b) frequency domain

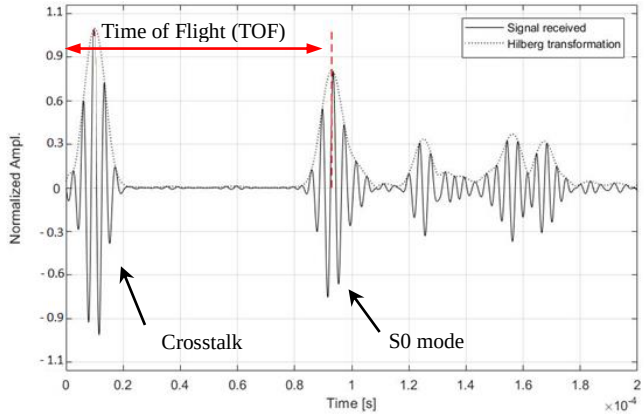

Figure 7: Extracting time of flight information

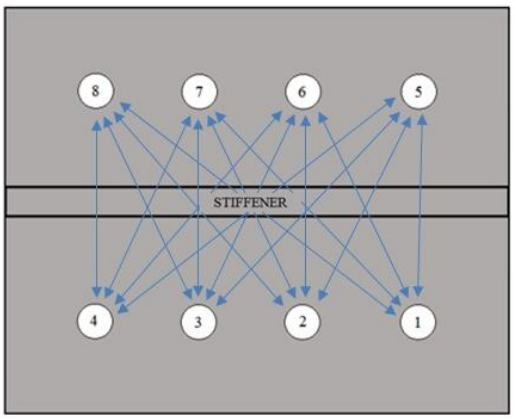

Figure 8: Different ways of stiffener in the signal.

2.3 Data processing

Group velocities for the symmetric mode (*S0*) are obtained by measuring the arrival time of the waves in flat panel for all PZT ways. The velocities obtained for a frequency range between 150 kHz and 500 kHz are shown in Fig. 9. The time of the wave to arrive is calculated with the group velocity. To do so, the Hilbert transformation of the signal is calculated as shown in Fig. 10.

DOI: 10.13009/EUCASS2019-565

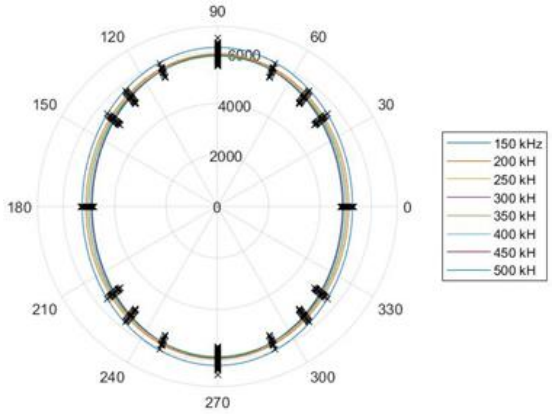

Figure 9: Polar plot of *S0* velocities for frequency range (150 - 500) kHz in all fibre directions

Two different effects can be observed in the signal through the stiffener: amplitude attenuation and signal time delay (Fig. 10). In order to have a complete dataset to analyze both effects, all the possible PZT ways throw the stiffener have been analyzed as shown in Fig. 8.

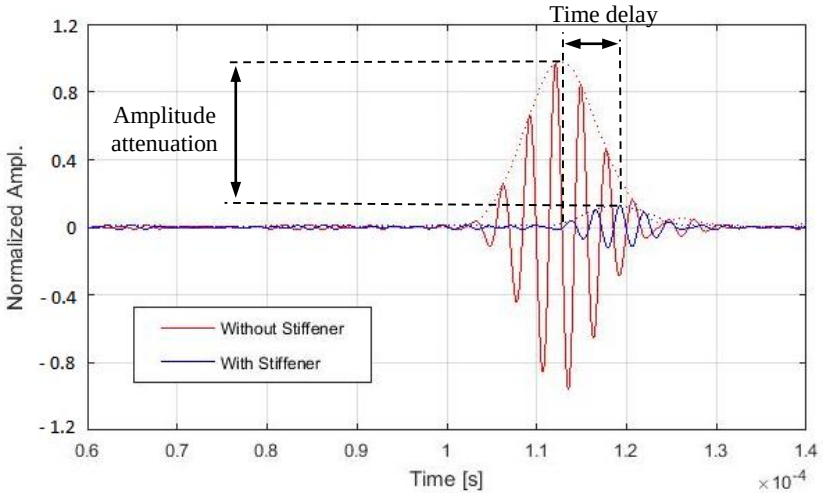

Figure 10: Amplitude attenuation and time delay due to the stiffener (PZT 1 to PZT 8 at 350 kHz).

It has been proven that the higher the frequency the lower retardation of the wave to arrive. This effect has a relation with the direction-dependent speed and the pulse of the signal chosen for these tests. It has been proven that the effect of the stiffener increases significantly the amplitude attenuation.

The accurate knowledge of wave velocity is required to perform an accurate damage location. Even if the amplitude attenuation and time delay promoted by the stiffener presence are not desirable, both issues keep stable in the *S0* mode signal at the different measurement paths allowing the signal processing with SHM purposes. In general, for the measurement equipment configuration employed in these tests, just one single stringer can be overpassed by a lamb wave.

2.4 Damage index (DI)

S0 and *A0* modes have important information about the health status of the structure such delaminations [6]. If the energy of the *S0* mode is meassured and compared to a reference status (non damaged structure), a damage index is then obtained for each single path of the Lamb wave. The damage index is defined as the relative ratio of the scatter energy contained in the *S0* mode wave packet [7].

The energy of the *S0* mode is obtained by meassuring its voltage area in the time domain as show in Eq. (3). This area is numerically calculated applying the Simpson's rule to the absolute value of the Hilbert transformation of the raw signal. The intregration bounds are set far enough from the *S0* peak that produce a change in the second derivated of

DOI: 10.13009/EUCASS2019-565

the signal, see Fig. 11. This has been inmplemented in an algorithm to calculate the energies for the 560 possible signal paths in multiple simulated damage possitions.

$$S_0 = \int_{t_i}^{t_f} H_{S0(t)}\, dt \tag{3}$$

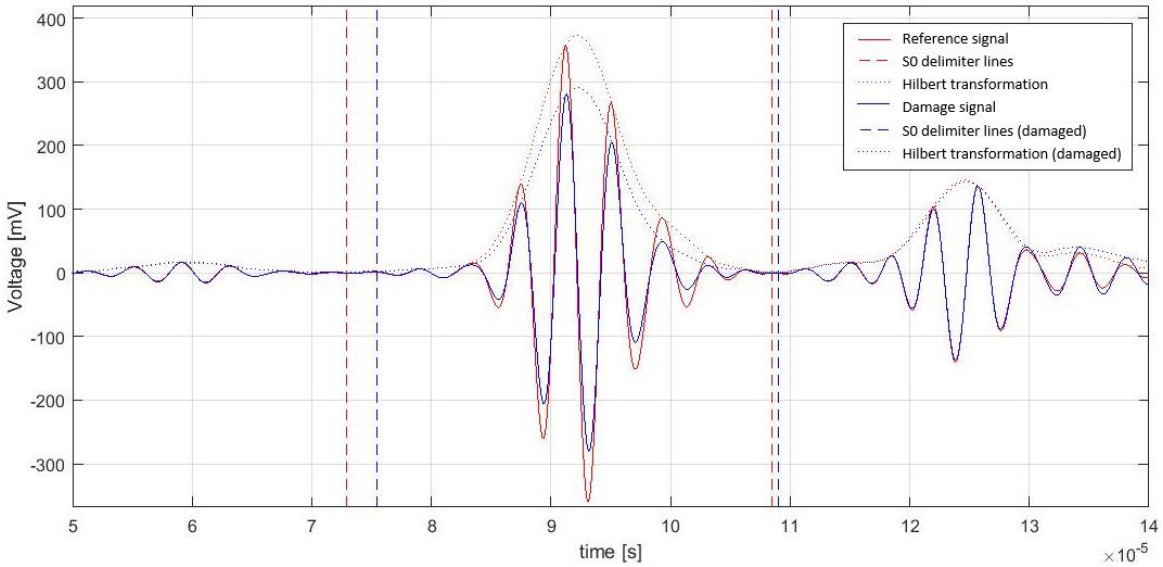

Figure 11: S0 mode.

DI can be calculated as shown in Eq. (4), where $H_{S0(t)\,ref}$ and $H_{S0(t)\,damaged}$ are the *S0* modes in the time domain for the reference and damaged signals respectively, α is a dimensionless indicator and t_i and t_f are the *S0* bounds. For this experiment, α value is set to 0.63, as the value that better fits the experimental results.

$$DI = \left(\frac{\int_{t_i}^{t_f} \left(H_{S0(t)\,ref} - H_{S0(t)\,damaged} \right)^2 dt}{\int_{t_i}^{t_f} H_{S0(t)\,ref}\, dt} \right)^{\alpha} \tag{4}$$

DI is then calculated for all the paths and its values are distributed in a Finit Element model of the plate. This distribution is arranged in a $(n\ x\ m)$ element array. The value of each element is calulated as the sumatory of the DIs for each frequency in its correspondant position. The elements affected in each path are the elements affected by the path line between the sensors as a function of the element array size $[n\ x\ m]$, see Fig. 12.a.

Damages have been simulated pasting a removable 15g vacum paste mass in different positions as shown in Fig 12.b. The results for a 100 x100 lement size array are shown in in Fig 13.

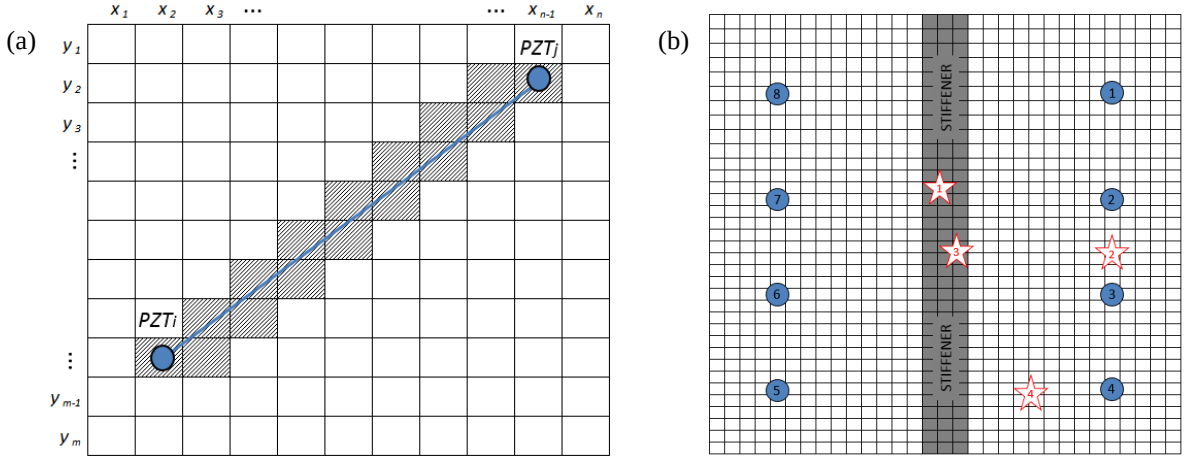

Figure 12: (a) Grid model for a damage position calculation using DI and (b) position for 4 simulated damages.

DOI: 10.13009/EUCASS2019-565

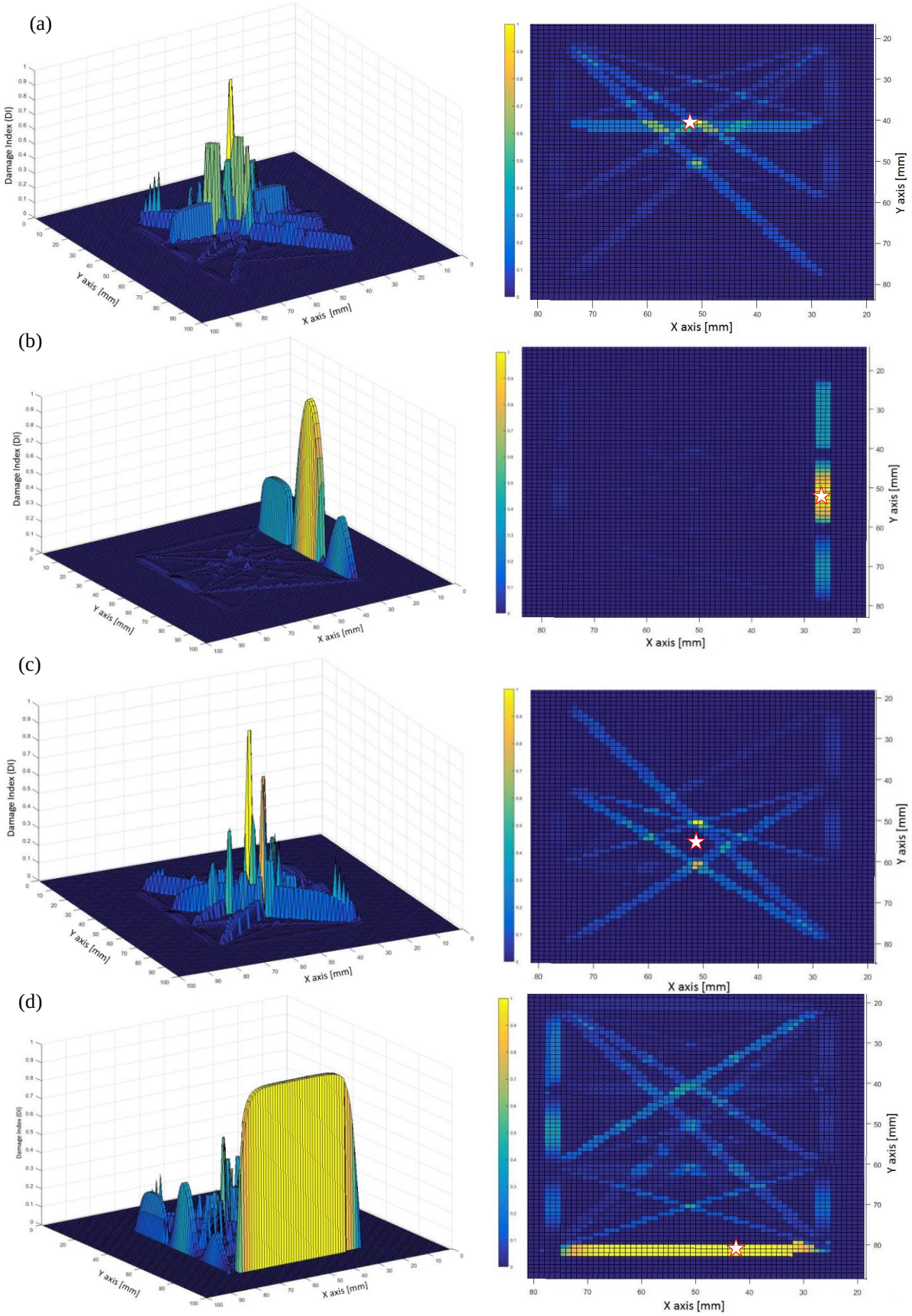

Figure 13: DI map plot results for 4 different simulated damages.

DOI: 10.13009/EUCASS2019-565

3. Passive monitoring

A second set of tests were carried out to predict the impact location for low energy impacts. Many different algorithms have been proposed for detecting the point of impact in non-isotropic composite plates. As proposed in [9], [10] and [11], the most common algorithm is based on the time of arrival of waves at the sensors, that requires to know the wave propagation velocity. If the velocity field is very uncertain due to a complex structure geometry, other techniques such the proper orthogonal decomposition [12], or the use of Neuronal Networks can produce good results.

For this experiment, the propagation velocity field trough the stiffener has been characterized and good results have been obtained using the already proposed triangulation techniques knowing the accurate TOF velocity field.

3.1 Experimental setup

A total of 64 impacts distributed in 78x78 mm square areas have been measured for a low energy level of 0.038 J as shown in Fig. 14.a. and Fig. 14.b. Impacts have been induced using a gravity impact test with the metallic ball shown in Fig. 14.c. Acquisition has been recorded at 200 ksps using a 16 bits DAQ resolution device. All the impacts were induced at the centroid position of each position over the grid distribution.

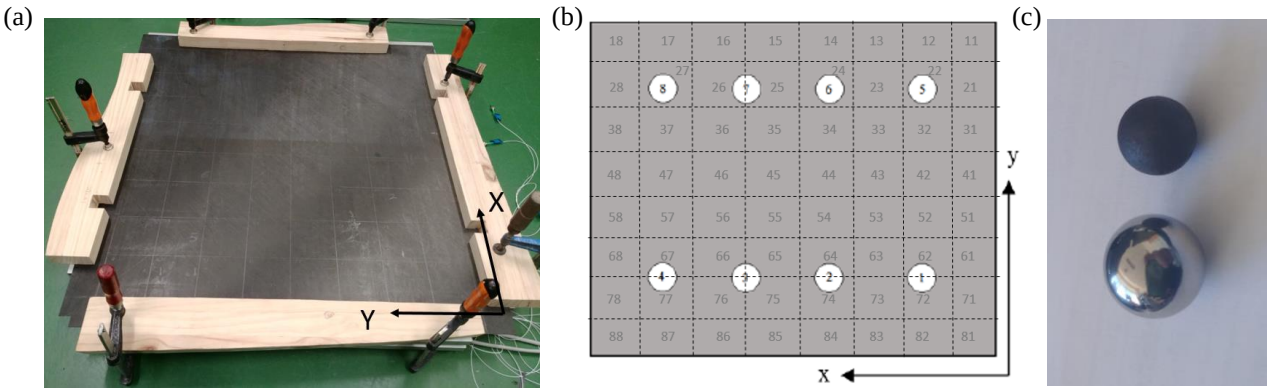

Figure 14: (a), (b) Grid distribution for the non-isotropic plate without stiffener and (c) impact metallic balls.

3.2 Signal treatment and impact location prediction

Before any signal treatment, electrical noise has been previously removed applying a Savitzky Golay filter to the time domain signal (Fig 15.b), implementing a change in the order and window size of the filter due to the frequency reduction of the elastic wave over time (Fig. 15.a). Once the noise is removed, wave arrival times have been calculated detecting a significant change in the standard deviation of the signal (Fig 16.b).

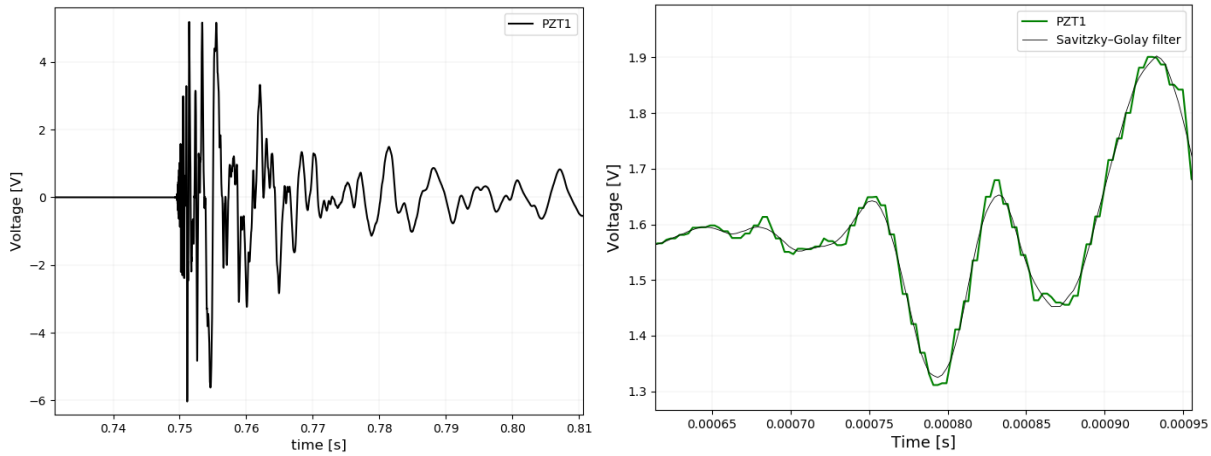

Figure 15: (a) Impact signal in time domain and (b) filtered signal applied to the first arrival wave.

The sensor position coordinates are defined as $[x_i, y_i]$, where i takes the value of each sensor (from 1 to 8) and the impact position to guess is defined as $[x_0, y_0]$. The arrival times are defined as t_i, setting to zero the first arrival time

DOI: 10.13009/EUCASS2019-565

of each impact as a reference PZT sensor. Wave velocities ($v_{(\theta_i)}$) are direction dependent due to the quasi-isotropic properties and the effect of the stiffener. Velocities were experimentally calculated dividing the distance from the impact to each sensor by the correspondent time of arrival. As shown in Fig. 16.a, two different direction dependent velocity maps were obtained: for the flat areas without stiffener in the propagation path and for the flat areas with the stiffener in the propagation path.

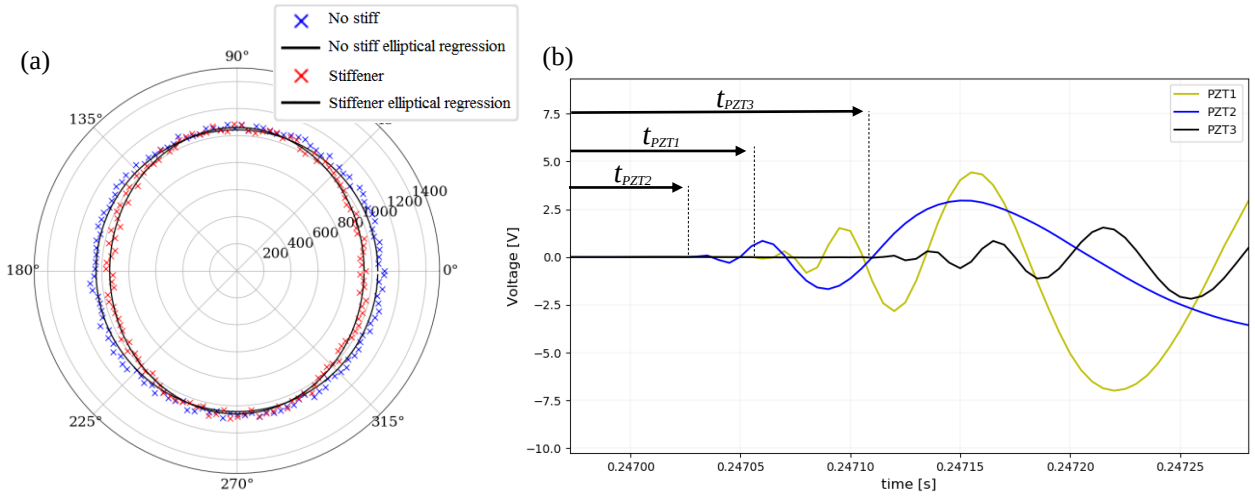

Figure 16: (a) Polar plot from experimental data and (b) arrival time calculation.

It has been observed that an ellipse approximation fits perfectly the experimental velocities obtained (Fig. 16.a). Eq. (6) represents the ellipse speed function taking V_x and V_y as the semi-minor and semi-major axes of the experimental data regression.

Table 1: Experimental velocity results (semi-major and semi-minor axis for the ellipses of Fig. 16.a)

	V_x [m/s]	V_y [m/s]
Flat panel (without stiffener)	1039	1046
Flat panel (with stiffener)	911	1030

The distance from the impact to each sensor is calculated in Eq. (5). Velocity dependent is calculated using the ellipse equation (Eq. (6)) for a given direction θ_i (Eq. (7)).

$$d_i = \sqrt{(x_0 - x_i)^2 + (y_0 - y_i)^2} = v_{(\theta_i)} t_i \tag{5}$$

$$v_{(\theta_i)} = \left(\frac{cos^2\theta_i}{V_x} + \frac{sin^2\theta_i}{V_y} \right)^{-1/2} \tag{6}$$

$$\theta_i = \tan^{-1}\left(\frac{y_i - y_0}{x_i - x_0} \right) \tag{7}$$

Once all the parameters are known, the target is to guess the impact position $[x_0, y_0]$ finding a way to solve Eq. (5), (6) and (7) for all *i* sensors. An algorithm proposed in [5], based on [6], to solve Eq. (5), (6) and (7), consist of obtaining the values of $[x_0, y_0]$ that minimize an error function. The error function (Eq. (8)) is calculated combing all possible time of arrival combinations from all sensor resulting on $n(n-1)/2$ possible combinations for *n* sensors.

DOI: 10.13009/EUCASS2019-565

$$E_{(x_0,y_0)} = \sum_{i=1}^{n-1} \sum_{j=i+1}^{n} \left(v_{(\theta_i)} v_{(\theta_j)} (t_i - t_j) - v_{(\theta_j)} \sqrt{(x_0 - x_i)^2 + (y_0 - y_i)^2} + v_{(\theta_i)} \sqrt{(x_0 - x_j)^2 + (y_0 - y_j)^2} \right)^2 \quad \textbf{(8)}$$

In this paper, two different methods have been included based on minimize $E_{(x_0,y_0)}$ from Eq.(8). The first one consist of minimize the error function taking all the possible combinations: $n = 8$; 28 sensor combinations; one single solution and low computational time. The second one consist of minimize the error function taking all possible 3 different sensor combinations: $n = 3$; 3 sensor combinations; 54 solutions, more computational time, taking the mean and median as results. As proposed in [5], Eq. (6), (7) and (8) have been implemented in an efficient algorithm to solve both methods applying a $[n\ x\ m]$ grid over the panel. The results for the impact position 34 are shown in Fig. 17.a. with its error funcion results over the grid map in Fig 17.b.

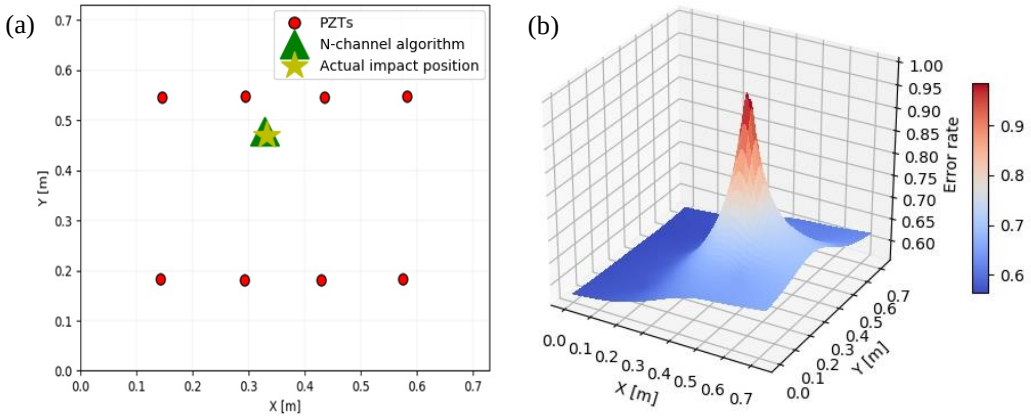

Figure 17: (a) Prediction results for impact position 53 using n = 8 sensor combinations and (b) error function results

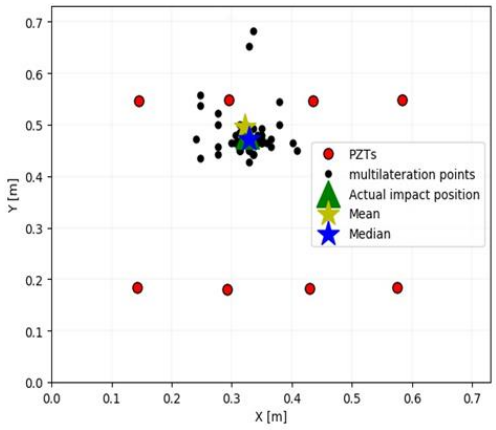

Figure 18: Mean and media prediction results for impact position 53 using n = 3 multi-combination

In Fig. 19, the dispersion reults (given as the differece in mm between the actual and predicted postion) are shown for all the impact positions over the panel with (Fig 19.a.) and without (Fig 19.b.) the stiffener.

DOI: 10.13009/EUCASS2019-565

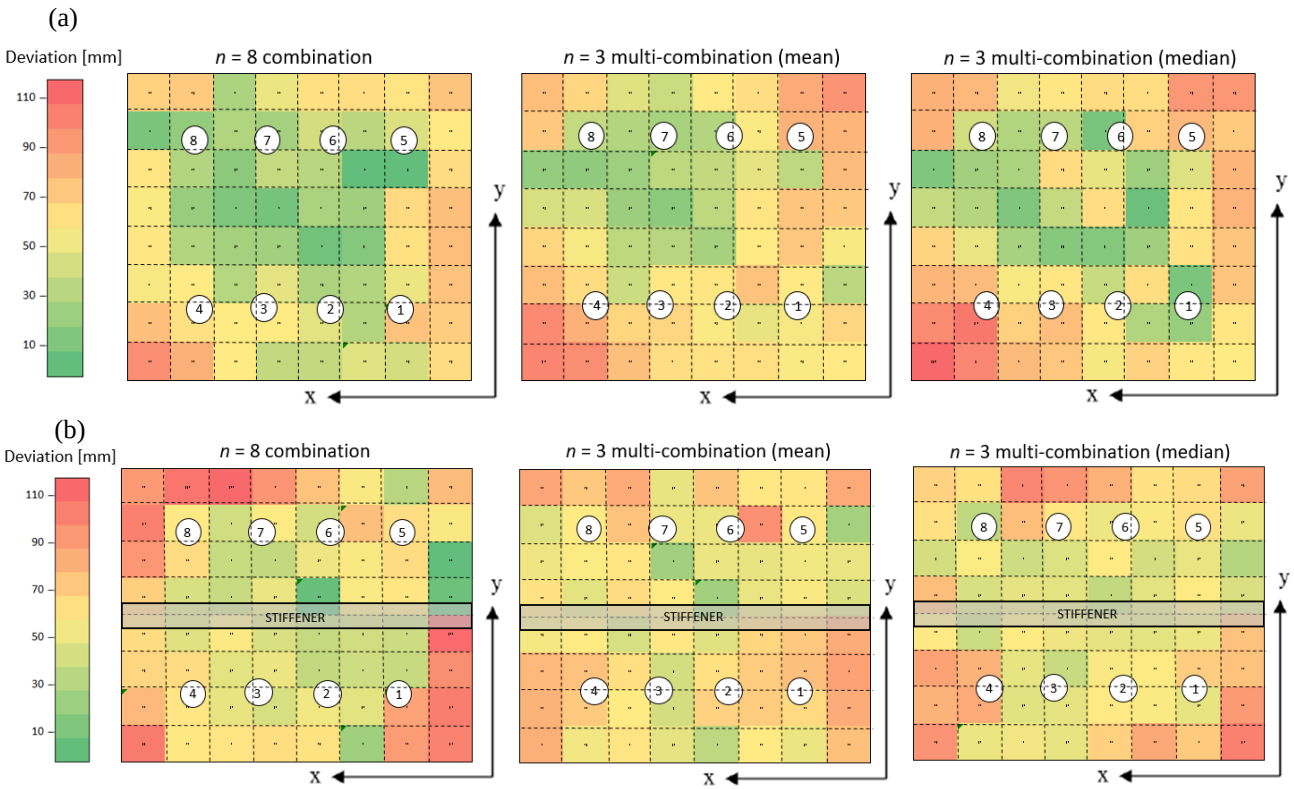

Figure 19: Deviation results of the impact prediction using

Conclusions

Lamb wave frequencies have to be carefully chosen for a better signal recognition through stiffener structures. T-shape stiffener thickness and geometry along with the wave energy emitted (selection of the proper frequency and pulse) plays an important role in the signal recognition for damage detection.

Good prediction results for low energy impact tests were obtained using time of arrival of waves at the sensors. The same accuracy results have been obtained using algorithms with different computational times, proven the less computational time algorithm as the most efficient one. It has also been observed that the effect of the stiffener reduces the accuracy when the time of arrival of waves increases. This effect can be smoothed with the implementation of a weight function over the longer time of arrivals in the error function. Other techniques such the use of neuronal networks could produce a lot better results increasing the preparation time and computational resources.

References

[1] Zhongqing Su et al, Guided Lamb waves for identification of damage in composite structures: A review, Journal of Sound and Vibration 295 (2006) 753–780.
[2] J.D. Achenbach, Wave Propagation in Elastic Solids, North-Holland, New York,1904.
[3] J.L. Rose, Ultrasonic Waves in Solid Media, Cambridge University Press, Cambridge, 1999.
[4] V. Giurgiutiu, Structural Health Monitoring with Piezoelectric Wafer Active Sensors, Academic Press, Amsterdam, 2008.
[5] Lamb, H. "On Waves in an Elastic Plate." Proc. Roy. Soc. London, Ser. A 93, 114–128, 1917.
[6] Takahiro Hayashi and Koichiro Kawashima, Multiple reflections of Lamb waves at a delamination, Ultrasonics 40 (2002) 193–197.
[7] J-B and Chang, F-K, (2004. Ultrasonic non-destructive evaluation for structural health monitoring: built-in diagnostics for hot-spot monitoring in metallic and composite structures. Chapter 9 in Ultrasonic Nondestructive Evaluation Engineering and Biological Material Characterization, edited by Kundu T. CRC Press, NY.
[8] Jeong-Beom Ihn and Fu-Kuo Chang, Detection and monitoring of hidden fatigue crack growth using a built-in piezoelectric sensor/actuator network: I. Diagnostics, Smart Mater. Struct. 13 609.
[9] Talieh Hajzargerbashi, Tribikram Kundu and Scott Bland. An improved algorithm for detecting point of impact in anisotropic inhomogeneous plates. Ultrasonics 51 (2011) 317–324.

DOI: 10.13009/EUCASS2019-565

[10] T. Kundu, S. Das, K.V. Jata, Point of impact prediction in anisotropic fiber reinforced composite plates from the acoustic emission data, review of progress in quantitative nondestructive evaluation, American Institute of Physics (2007).
[11] Tribikram Kundu et al, Locating point of impact in anisotropic fiber reinforced composite plates, Ultrasonics 48 (2008) 193–201.
[12] M. Thienea, U. Galvanetto. Impact location in composite plates using proper orthogonal decomposition. Mechanics Research Communications 64 (2015) 1–7.